Multi-Beam Synthesis of Linear Phased Array - A Numerical Assessment

P. Rocca, N. Anselmi, M. A. Hannan and A. Massa

Contents

1 Numerical Assessment - Linear Array Synthesis

1.1 $P = 5$, $\theta_1 = 79.06\,deg$, $\theta_2 = 84.93\,deg$, $\theta_3 = 90.75\,deg$, $\theta_4 = 96.57\,deg$, $\theta_5 = 102.46\,deg$

The test case has been performed using the parameters below.

Parameter	*Values*					
γ_a	0.100	0.309	0.954	2.947	9.103	
	10.985	33.932	104.811	323.746	1000.000	
γ_b	0.0001	0.00054	0.00295	0.01600	0.08685	
	0.47149	2.55955	13.89495	75.43120	100.00000	
Pattern Samples, K	22	24	26	28	30	32
	34	36	38	40	42	44
Aperture Samples, N	500	600	700	800	900	1000
Noise Variance, σ	0.000010	0.000031	0.000095	0.000295	0.000910	
	0.002812	0.008685	0.026827	0.082864	0.100000	

Table I: Simulation Parameters

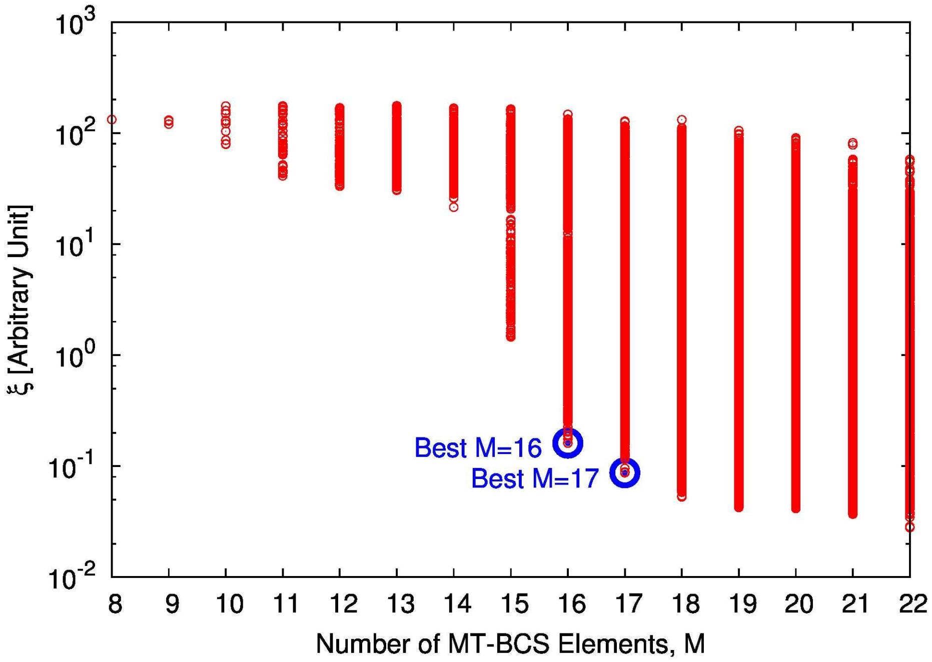

Figure 1: Output solutions from MT-BCS procedure

*Fig.*1 shows the solutions of the MT-BCS procedure having number of elements $M \leq 22$. The y-axis represents the mean error between the reference power patterns and the power pattern at the output of the MT-BCS.

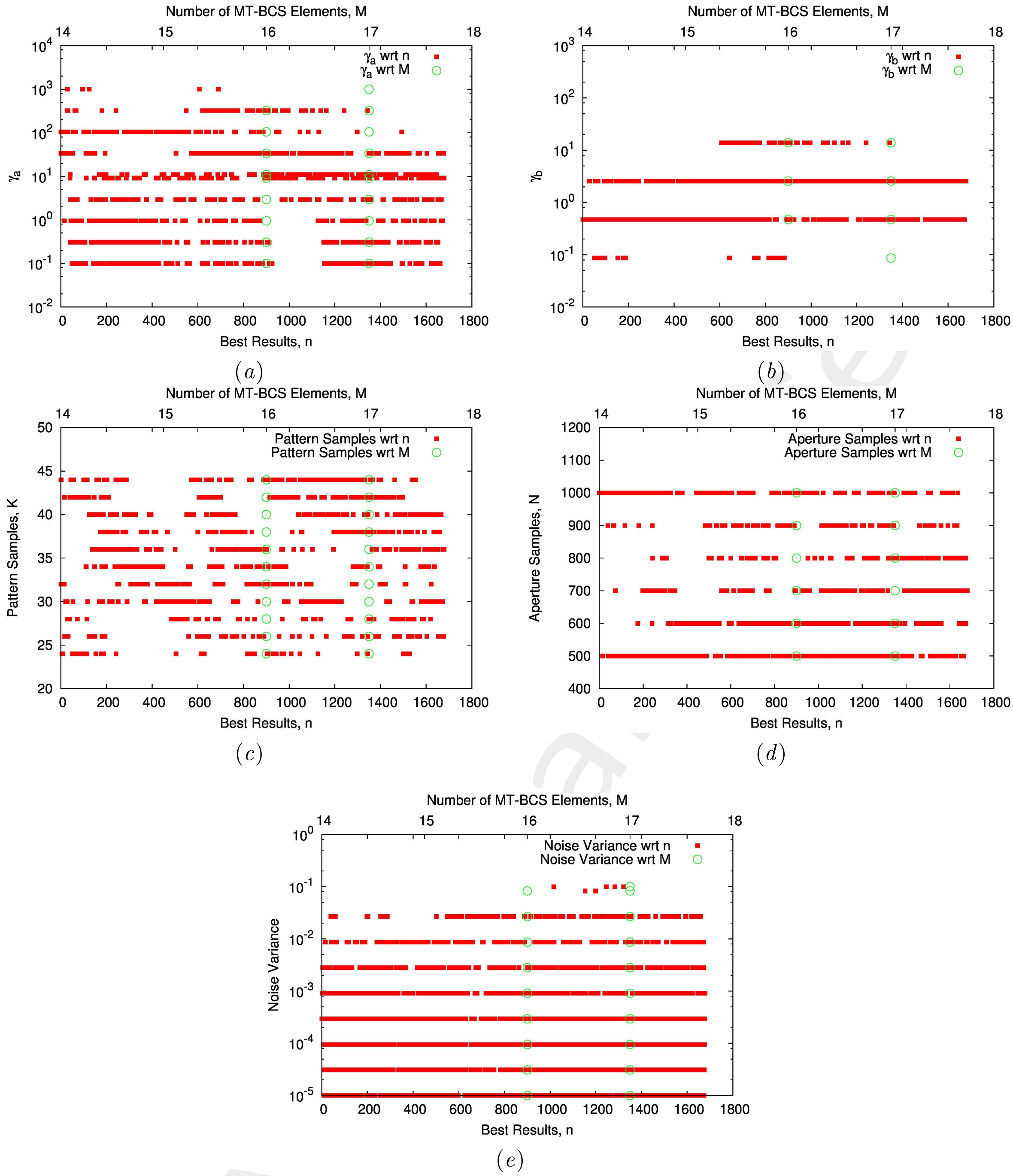

Figure 2: Parameters distribution, (a) γ_a, (b) γ_b, (c) *Pattern Samples,* (d) *Aperture Samples,* (e) *Noise Variance*

Fig.2 shows parameter distributions as function of "Best Results" (the ones with error value under $8.0 \times 10^{-1}$and number of MT-BCS elements lower than 18, sorted by error value) and number of elements.

As for case $P = 3$, $\theta_1 = 84.93\,deg$, $\theta_2 = 90.75\,deg$, $\theta_3 = 96.57\,deg$ that there are no "Best Results " with $M = 15$ number of MT-BCS elements as shown in *Fig.2* .

1.1.1 Solution: Best $M = 16$

γ_a	γ_b	*Pattern Samples [K]*	*Aperture Samples [N]*	*Noise Variance*
323.746	2.55955	24	1000	0.00001

Table II: MT-BCS Input Parameters

In *Tab.II* are reported MT-BCS parameters of solution Best $M = 16$. *Fig.3* shows elements positions of MT-BCS sparse linear array obtained from solution Best $M = 16$.

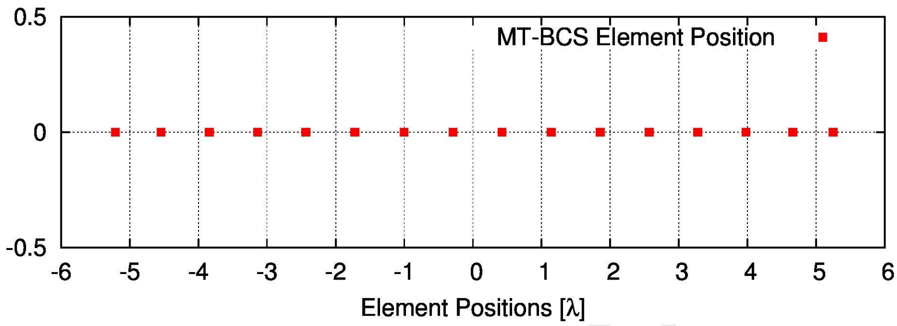

Figure 3: MT-BCS array elements positions

Pattern $\theta_1 = 79.06\,deg$

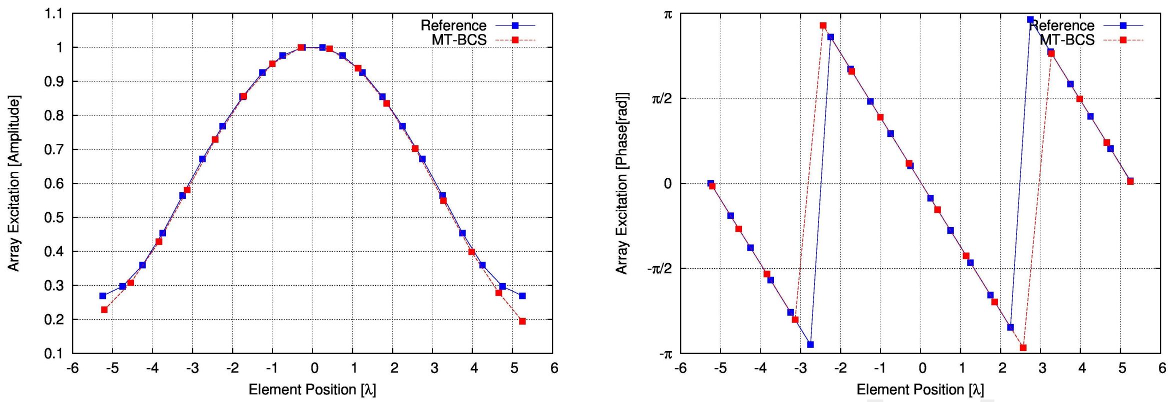

(a) (b)

Figure 4: Array excitations, (a)Amplitudes, (b)Phases

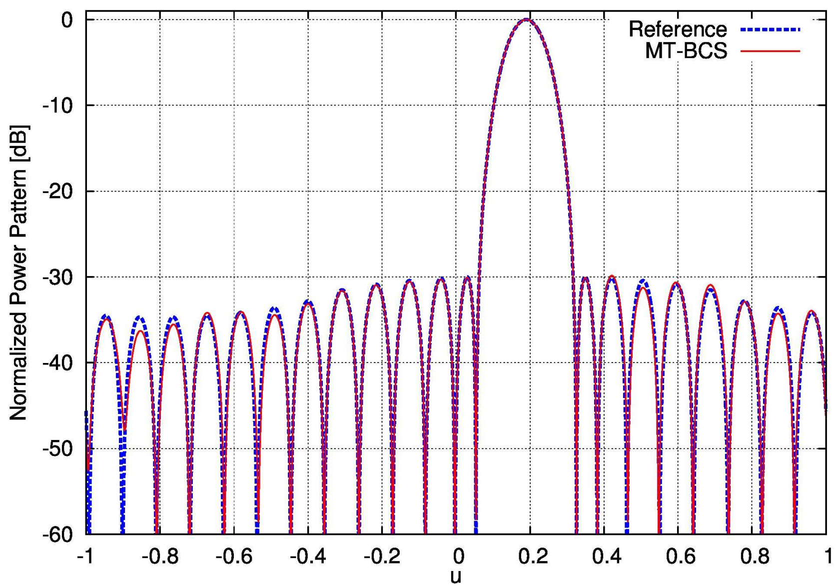

Figure 5: Power pattern comparison

Fig.4(a), *4*(b) show comparison between Reference and MT-BCS amplitudes and phases excitations respectively. *Fig.5* shows the comparison between Reference and MT-BCS power pattern for the steereng angle $\theta_1 = 79.06$ degrees.

	$SLL\,[dB]$	$D\,[dB]$	$HPBW\,[deg]$	M	err_1
$Reference$	-29.99	12.77	5.92	22	$-$
$MT-BCS$	-29.84	12.76	5.94	16	1.6056108×10^{-1}

Table III: Pattern $\theta_1$performance

In *Tab.*III comparison between Reference and MT-BCS power pattern performance parameters.

Pattern $\theta_2 = 84.93\, deg$

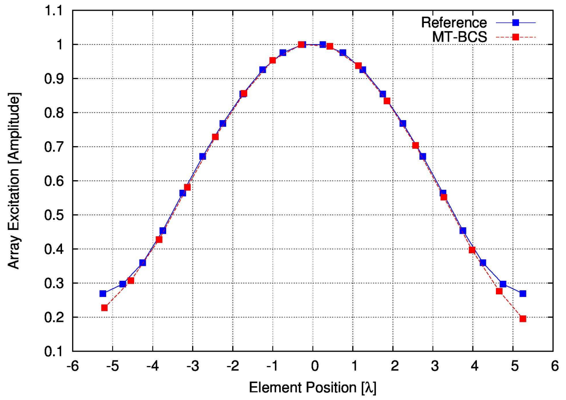

(a)

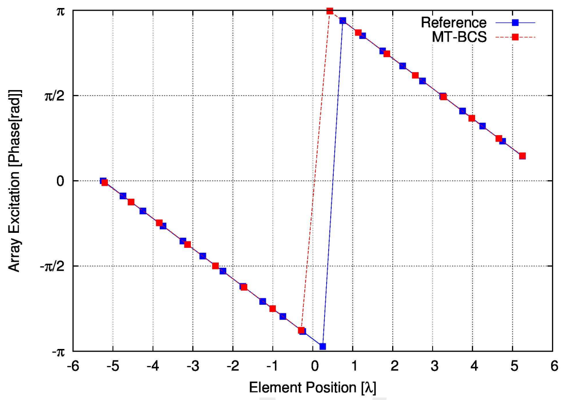

(b)

Figure 6: Array Excitations, (a)Amplitudes, (b)Phases

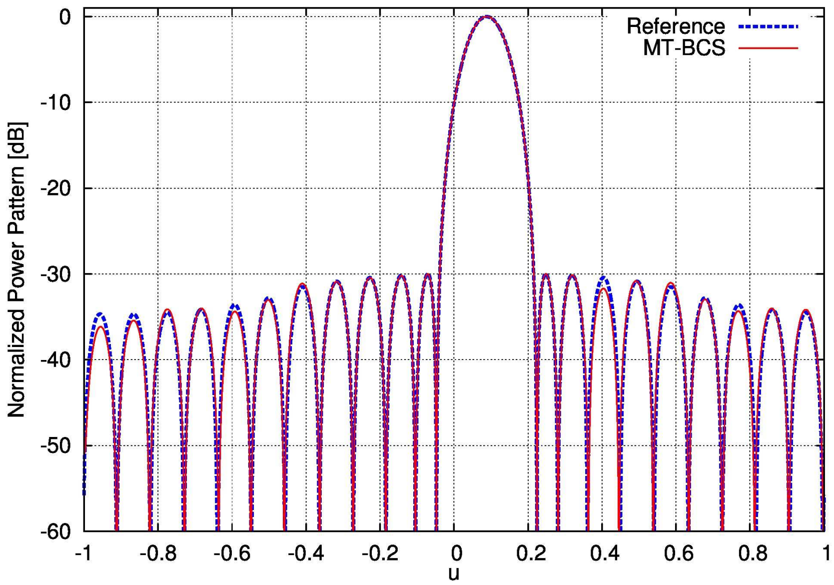

Figure 7: Power pattern comparison

Fig.6(a), $6(b)$ show comparison between Reference and MT-BCS amplitudes and phases excitations respectively.

Fig.7 shows the comparison between Reference and MT-BCS power pattern for the steereng angle $\theta_2 = 84.93$ degrees.

	$SLL\,[dB]$	$D\,[dB]$	$HPBW\,[deg]$	M	err_2
$Reference$	-29.99	12.77	5.84	22	$-$
$MT-BCS$	-29.98	12.76	5.85	16	1.866828×10^{-1}

Table IV: Pattern $\theta_2$performance

In *Tab.*IV comparison between Reference and MT-BCS power pattern performance parameters.

Pattern $\theta_3 = 90.75\,deg$

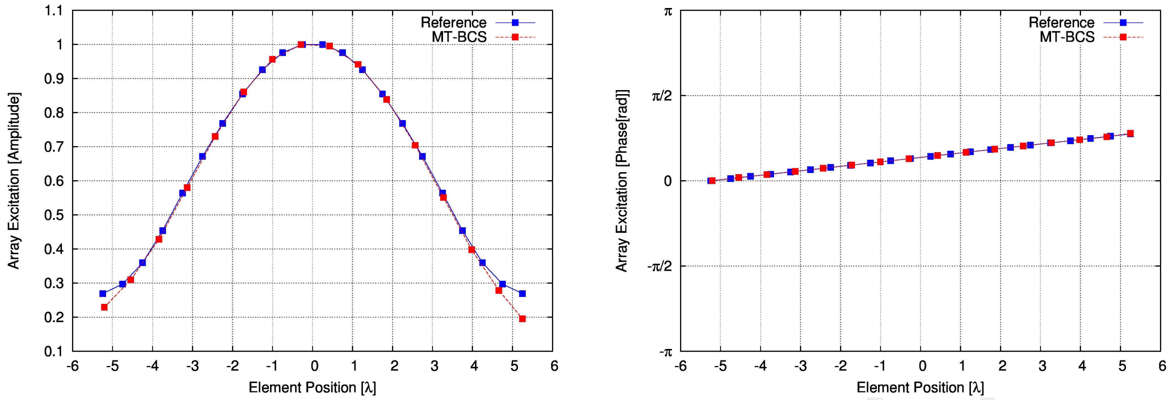

(a) (b)

Figure 8: Array Excitations, (a)Amplitudes, (b)Phases

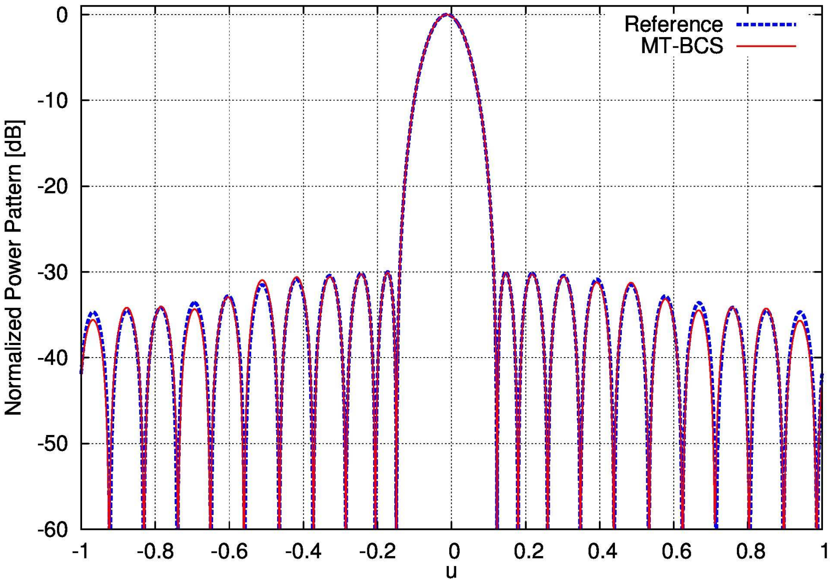

Figure 9: Power pattern comparison

Fig.8(a), *8*(b) show comparison between Reference and MT-BCS amplitudes and phases excitations respectively.

Fig.9 shows the comparison between Reference and MT-BCS power pattern for the steereng angle $\theta_3 = 90.75$ degrees.

	$SLL\,[dB]$	$D\,[dB]$	$HPBW\,[deg]$	M	err_3
$Reference$	-29.99	12.77	5.82	22	$-$
$MT-BCS$	-30.04	12.76	5.83	16	1.506719×10^{-1}

Table V: Pattern $\theta_3$performance

In *Tab.*V comparison between Reference and MT-BCS power pattern performance parameters.

Pattern $\theta_4 = 96.57\,deg$

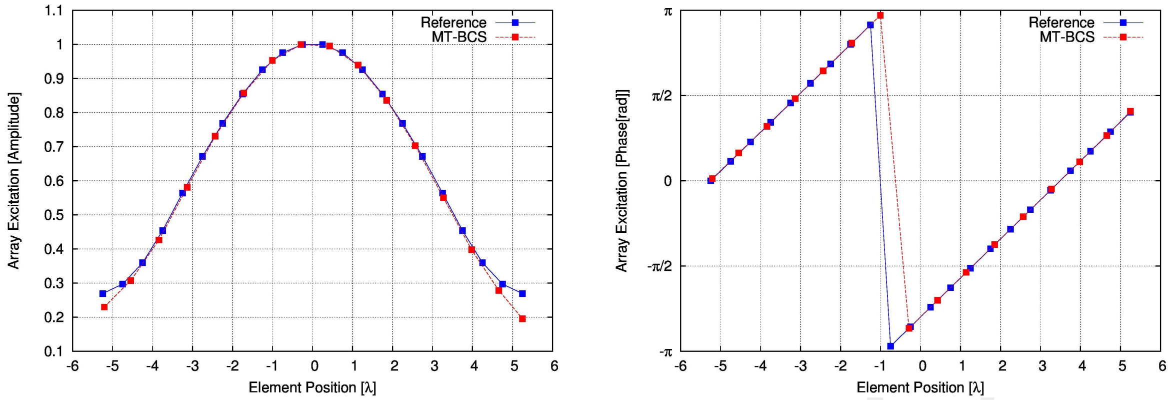

(a) (b)

Figure 10: Array Excitations, (a)Amplitudes, (b)Phases

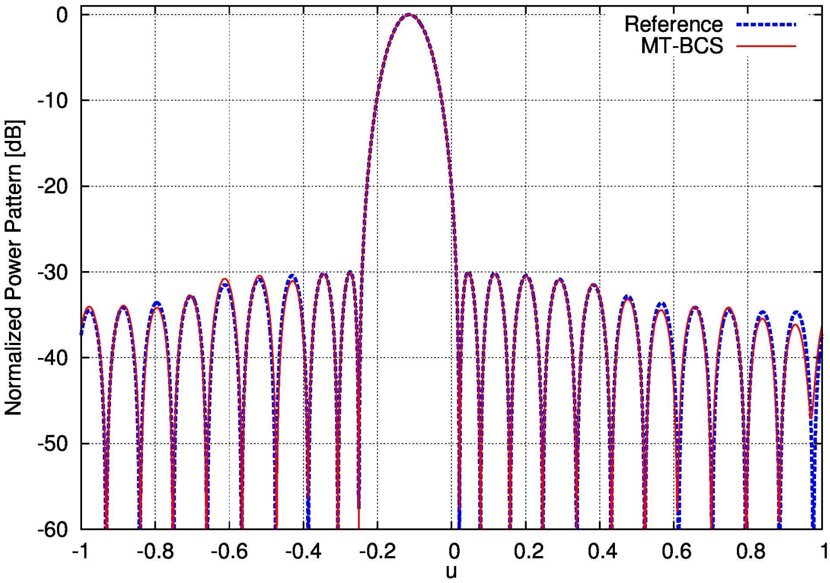

Figure 11: Power pattern comparison

Fig.10(a), *10*(b) show comparison between Reference and MT-BCS amplitudes and phases excitations respectively.

Fig.11 shows the comparison between Reference and MT-BCS power pattern for the steereng angle $\theta_4 = 96.57$ degrees.

	$SLL\,[dB]$	$D\,[dB]$	$HPBW\,[deg]$	M	err_4
$Reference$	-29.99	12.77	5.86	22	$-$
$MT-BCS$	-30.06	12.76	5.87	16	1.505978×10^{-1}

Table VI: Pattern $\theta_4$performance

In *Tab.*VI comparison between Reference and MT-BCS power pattern performance parameters.

Pattern $\theta_5 = 102.46\,deg$

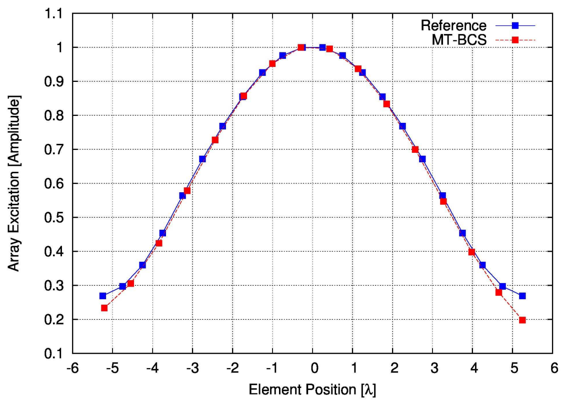

(a)

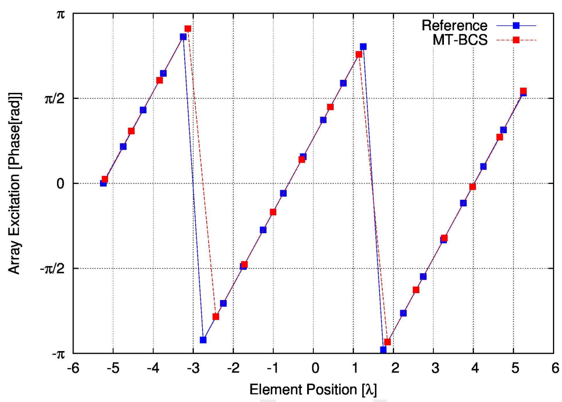

(b)

Figure 12: Array Excitations, (a)Amplitudes, (b)Phases

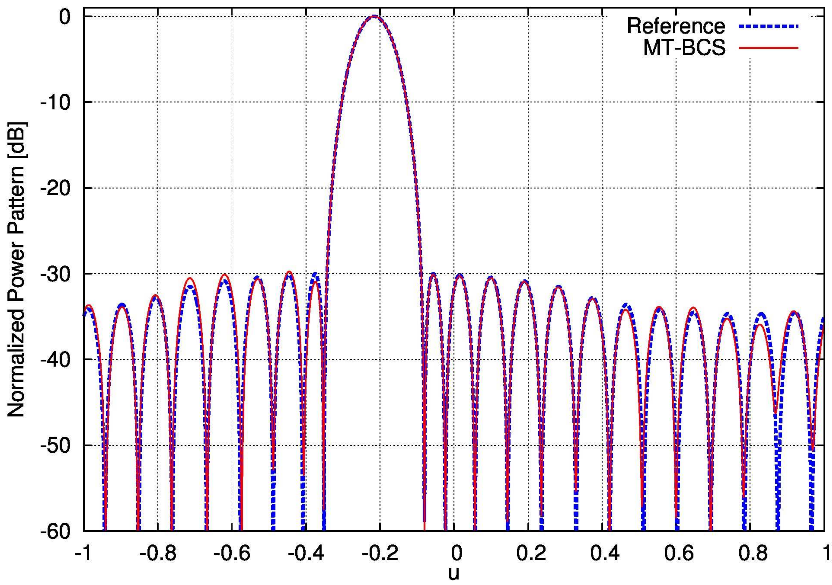

Figure 13: Power pattern comparison

Fig.12(a), *12*(b) show comparison between Reference and MT-BCS amplitudes and phases excitations respectively.

Fig.13 shows the comparison between Reference and MT-BCS power pattern for the steereng angle $\theta_5 = 102.46$ degrees.

	$SLL\,[dB]$	$D\,[dB]$	$HPBW\,[deg]$	M	err_5
$Reference$	-29.99	12.77	5.96	22	$-$
$MT-BCS$	-29.74	12.76	5.96	16	1.559504×10^{-1}

Table VII: Pattern $\theta_5$performance

In *Tab.*VII comparison between Reference and MT-BCS power pattern performance parameters.

1.1.2 MT-BCS errors

In *Tab.*VIII are reported the error values. In particular:

- I: total number of reference power pattern [I];
- ξ: total error of the entire procedure;
- err_i ($i = 1, \ldots, I$): error on sigular reference and MT-BCS pattern pair.

Solution	err_1	err_2	err_3	err_4	err_5
Best $M = 16$	1.605611×10^{-1}	1.866828×10^{-1}	1.506719×10^{-1}	1.505978×10^{-1}	1.559504×10^{-1}

Solution	I	ξ
Best $M = 16$	5	1.608928×10^{-1}

Table VIII: MT-BCS errors

1.2 $P = 6$, $\theta_1 = 79.06\,deg$, $\theta_2 = 84.93\,deg$, $\theta_3 = 90.75\,deg$, $\theta_4 = 96.57\,deg$, $\theta_5 = 102.46\,deg$, $\theta_6 = 108.47\,deg$

The test case has been performed using the parameters below.

Parameter	*Values*					
γ_a	0.100	0.309	0.954	2.947	9.103	
	10.985	33.932	104.811	323.746	1000.000	
γ_b	0.0001	0.00054	0.00295	0.01600	0.08685	
	0.47149	2.55955	13.89495	75.43120	100.00000	
Pattern Samples, K	22	24	26	28	30	32
	34	36	38	40	42	44
Aperture Samples, N	500	600	700	800	900	1000
Noise Variance, σ	0.000010	0.000031	0.000095	0.000295	0.000910	
	0.002812	0.008685	0.026827	0.082864	0.100000	

Table IX: Simulation Parameters

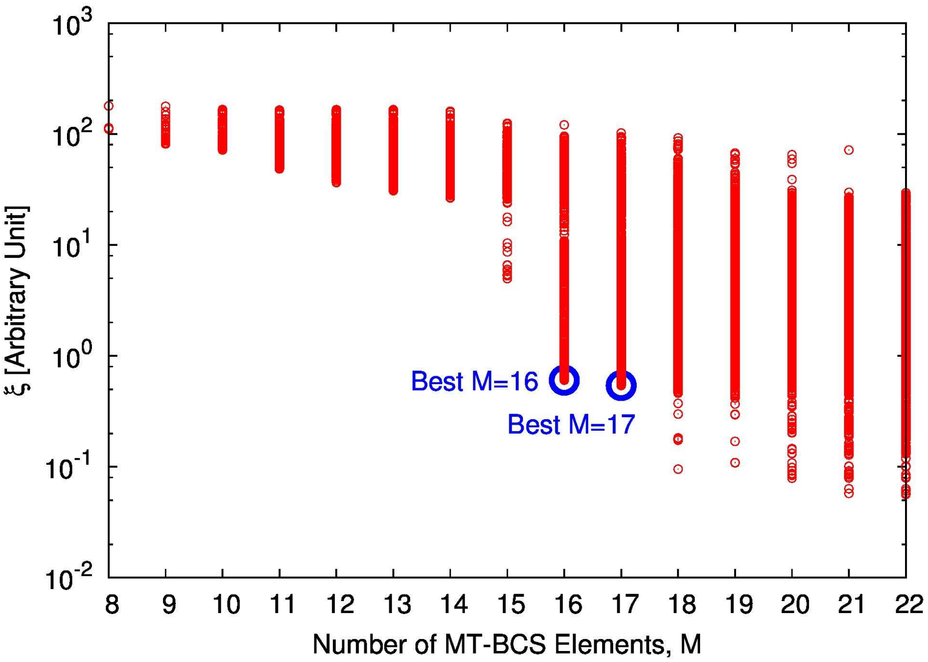

Figure 14: Output solutions from MT-BCS procedure

*Fig.*14 shows the solutions of the MT-BCS procedure having number of elements less than or equal to $M = 22$. The y-axis represents the mean error between the reference power patterns and the power pattern at the output of the MT-BCS.

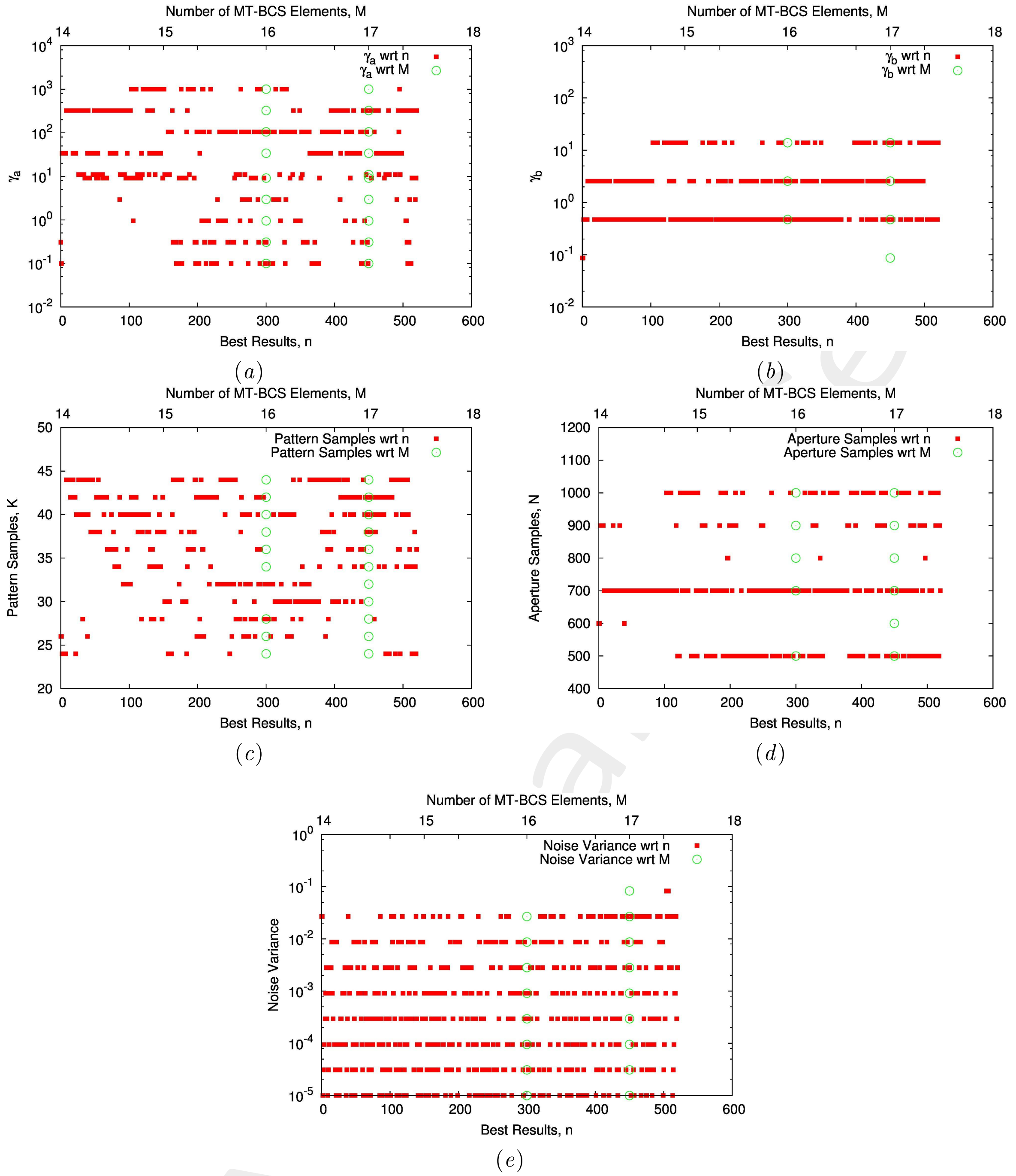

Figure 15: Parameters distribution, (a) γ_a, (b) γ_b, (c) *Pattern Samples*, (d) *Aperture Samples*, (e) *Noise Variance*

Fig.15 shows parameter distributions as function of "Best Results" (the ones with error value under $8.0 \times 10^{-1}$and number of MT-BCS elements lower than 18, sorted by error value) and number of elements.

As for case $P = 3$, $\theta_1 = 84.93\,deg$, $\theta_2 = 90.75\,deg$, $\theta_3 = 96.57\,deg$ that there are no "Best Results " with $M = 15$ number of MT-BCS elements as shown in *Fig.15* .

1.2.1 Solution: Best $M = 16$

γ_a	γ_b	*Pattern Samples [K]*	*Aperture Samples [N]*	*Noise Variance*
1000.000	13.8949	42	1000	0.002812

Table X: MT-BCS Input Parameters

In *Tab.X* are reported MT-BCS parameters of solution Best $M = 16$. *Fig.16* shows elements positions of MT-BCS sparse linear array obtained from solution Best $M = 16$.

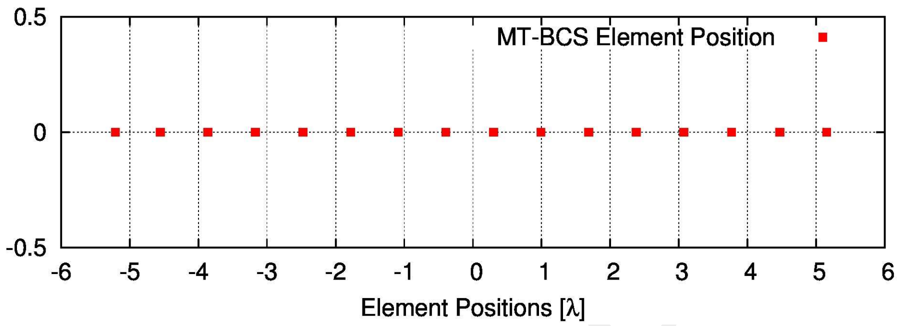

Figure 16: MT-BCS array elements positions

Pattern $\theta_1 = 79.06\,deg$

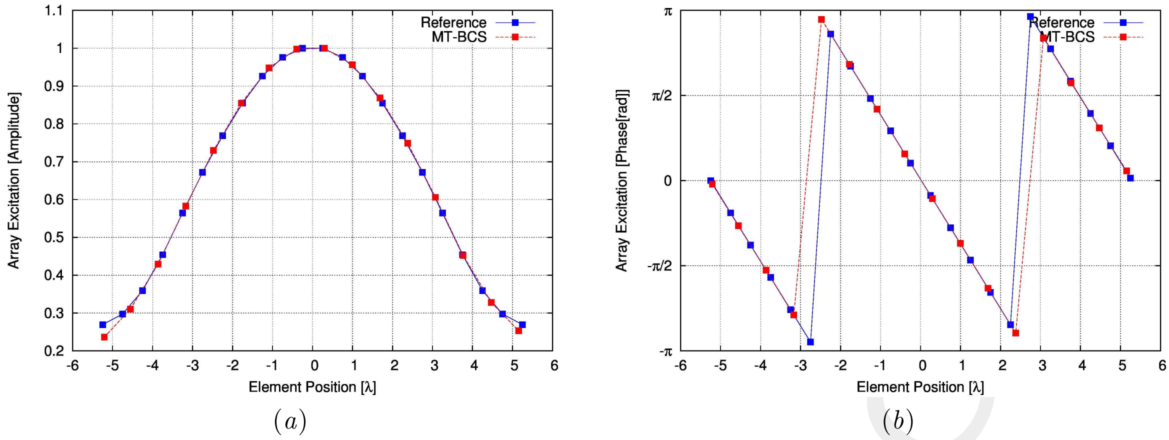

Figure 17: Array excitations, (a)Amplitudes, (b)Phases

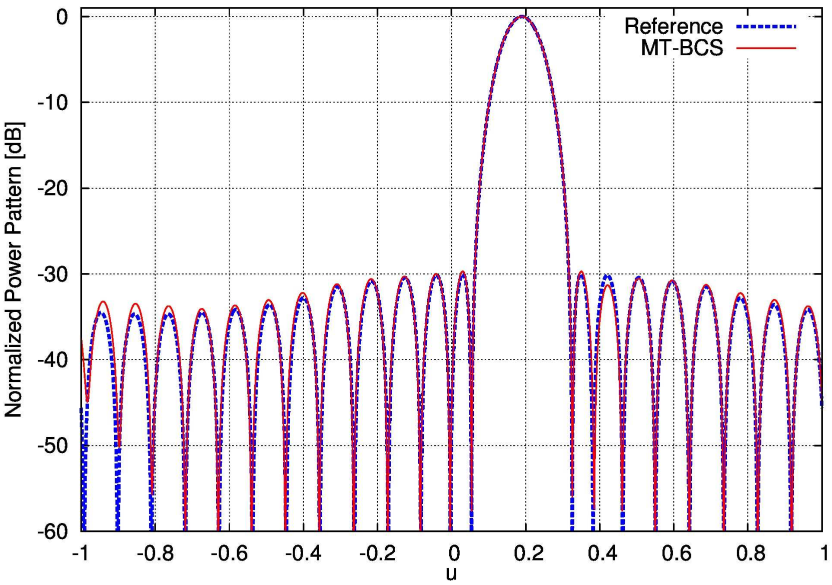

Figure 18: Power pattern comparison

Fig.17(a), *17*(b) show comparison between Reference and MT-BCS amplitudes and phases excitations respectively.

Fig.18 shows the comparison between Reference and MT-BCS power pattern for the steereng angle $\theta_1 = 79.06$ degrees.

	$SLL\,[dB]$	$D\,[dB]$	$HPBW\,[deg]$	M	err_1
$Reference$	-29.99	12.77	5.93	22	$-$
$MT-BCS$	-29.68	12.73	5.95	16	4.677504×10^{-1}

Table XI: Pattern $\theta_1$performance

In *Tab.*XI comparison between Reference and MT-BCS power pattern performance parameters.

Pattern $\theta_2 = 84.93\, deg$

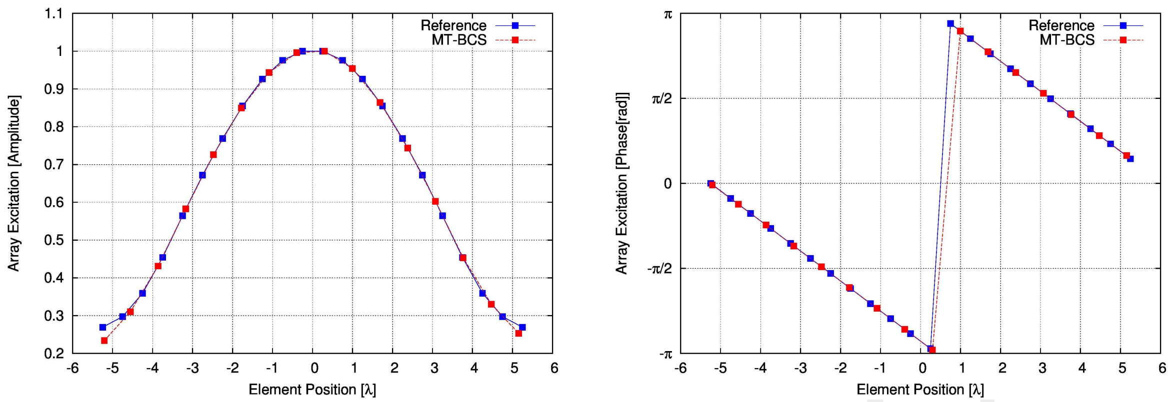

(a) (b)

Figure 19: Array Excitations, (a)Amplitudes, (b)Phases

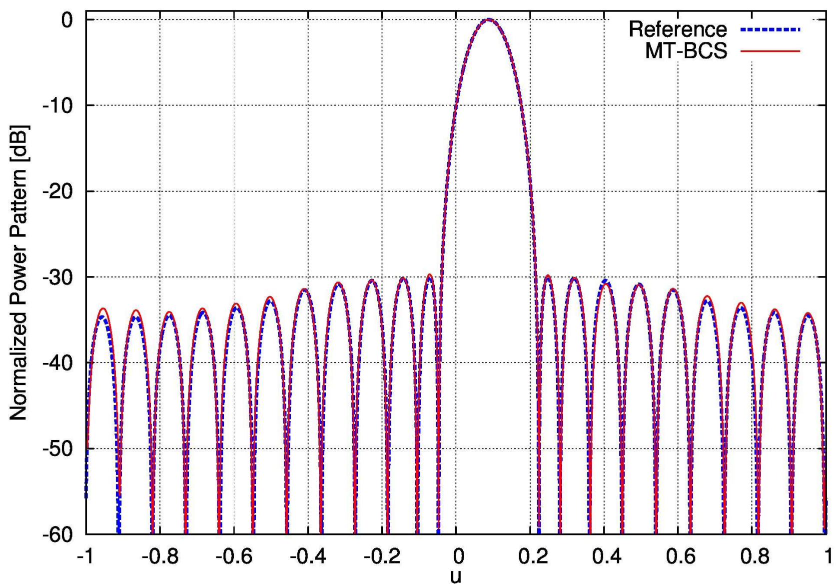

Figure 20: Power pattern comparison

Fig.19(a), *19*(b) show comparison between Reference and MT-BCS amplitudes and phases excitations respectively.

Fig.18 shows the comparison between Reference and MT-BCS power pattern for the steereng angle $\theta_2 = 84.93$ degrees.

	$SLL\,[dB]$	$D\,[dB]$	$HPBW\,[deg]$	M	err_2
$Reference$	-29.99	12.77	5.84	22	$-$
$MT-BCS$	-29.69	12.74	5.86	16	3.633513×10^{-1}

Table XII: Pattern $\theta_2$performance

In *Tab.*XII comparison between Reference and MT-BCS power pattern performance parameters.

Pattern $\theta_3 = 90.75\,deg$

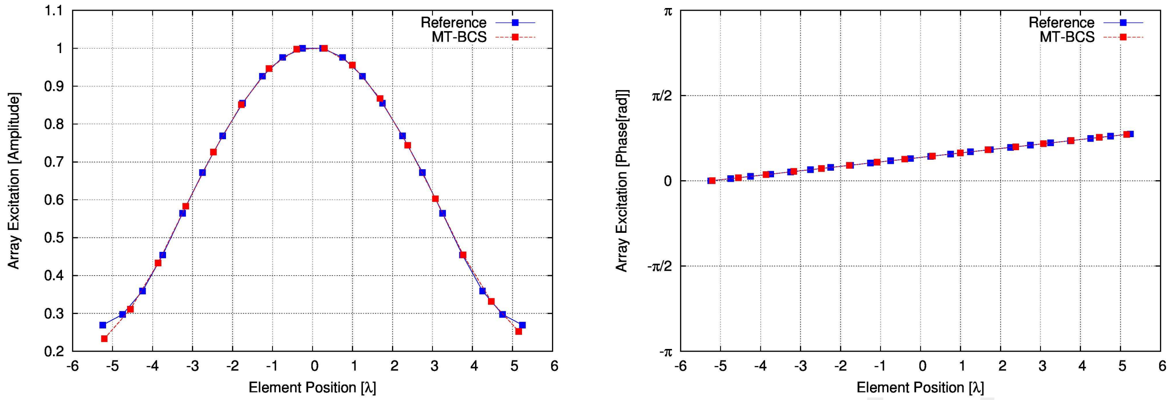

(a) (b)

Figure 21: Array Excitations, (a)Amplitudes, (b)Phases

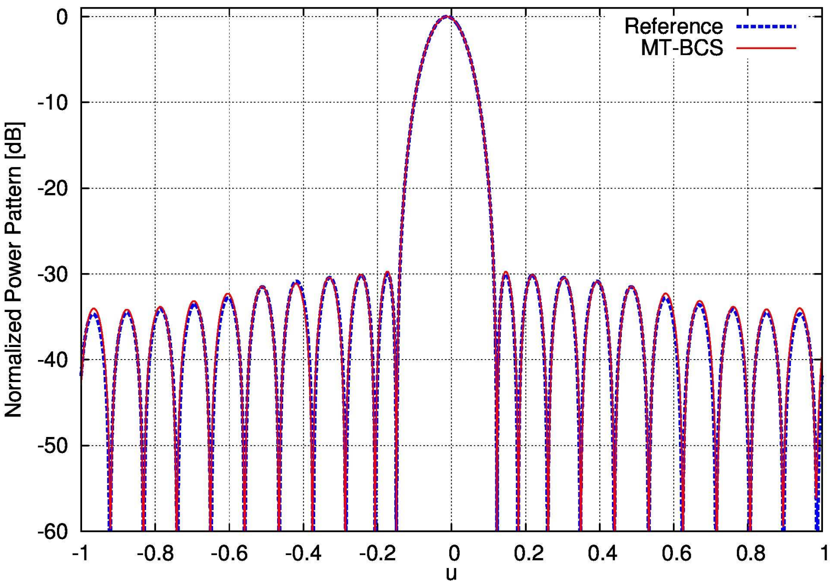

Figure 22: Power pattern comparison

Fig.21(a), *21*(b) show comparison between Reference and MT-BCS amplitudes and phases excitations respectively.

Fig.22 shows the comparison between Reference and MT-BCS power pattern for the steereng angle $\theta_3 = 90.75$ degrees.

	$SLL\,[dB]$	$D\,[dB]$	$HPBW\,[deg]$	M	err_3
$Reference$	-29.99	12.77	5.82	22	$-$
$MT-BCS$	-29.71	12.75	5.84	16	3.678745×10^{-1}

Table XIII: Pattern $\theta_3$performance

In *Tab.*XIII comparison between Reference and MT-BCS power pattern performance parameters.

Pattern $\theta_4 = 96.57\,deg$

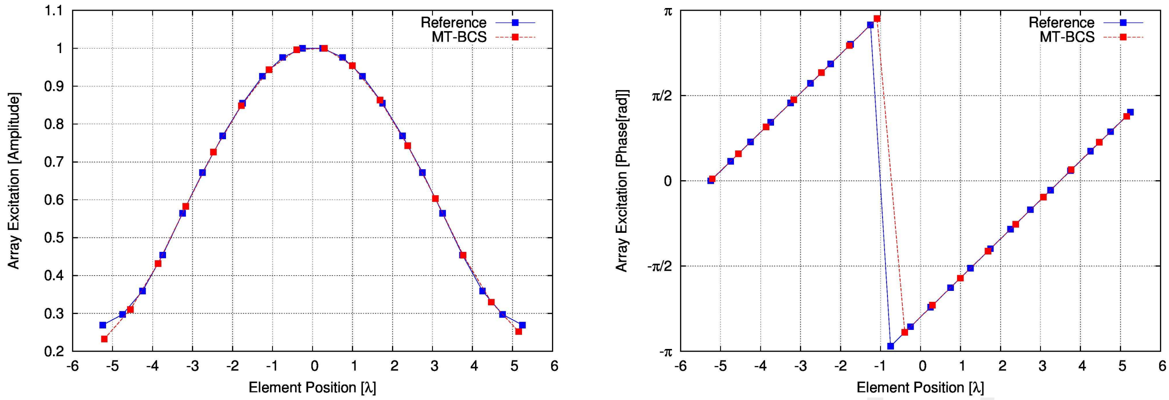

(a) (b)

Figure 23: Array Excitations, (a)Amplitudes, (b)Phases

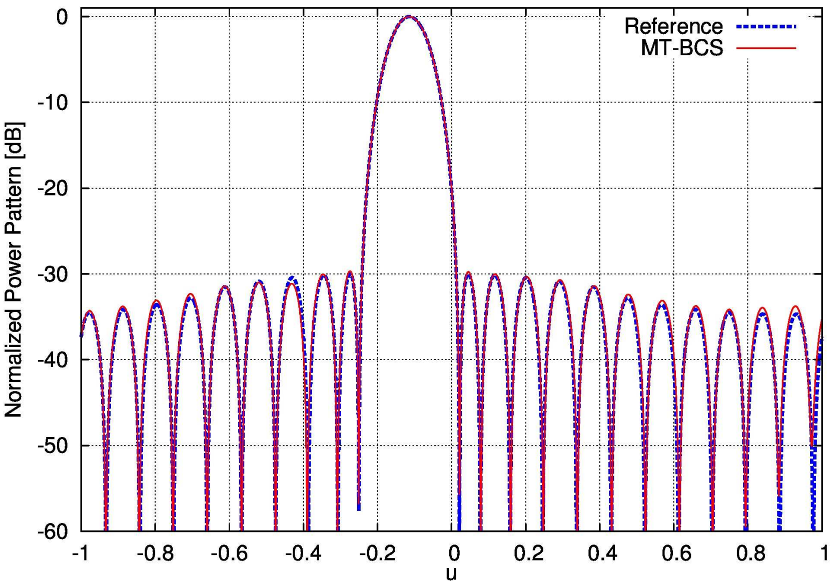

Figure 24: Power pattern comparison

Fig.23(a), *23*(b) show comparison between Reference and MT-BCS amplitudes and phases excitations respectively.

Fig.24 shows the comparison between Reference and MT-BCS power pattern for the steereng angle $\theta_4 = 96.57$ degrees.

	$SLL\,[dB]$	$D\,[dB]$	$HPBW\,[deg]$	M	err_4
$Reference$	-29.99	12.77	5.86	22	$-$
$MT-BCS$	-29.67	12.75	5.88	16	3.926148×10^{-1}

Table XIV: Pattern $\theta_4$performance

In *Tab.*XIV comparison between Reference and MT-BCS power pattern performance parameters.

Pattern $\theta_5 = 102.46\,deg$

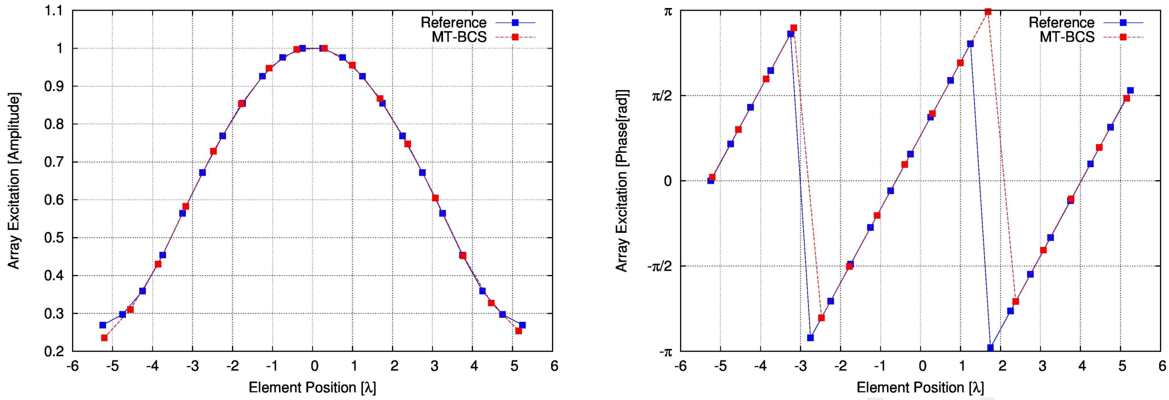

(a) (b)

Figure 25: Array Excitations, (a)Amplitudes, (b)Phases

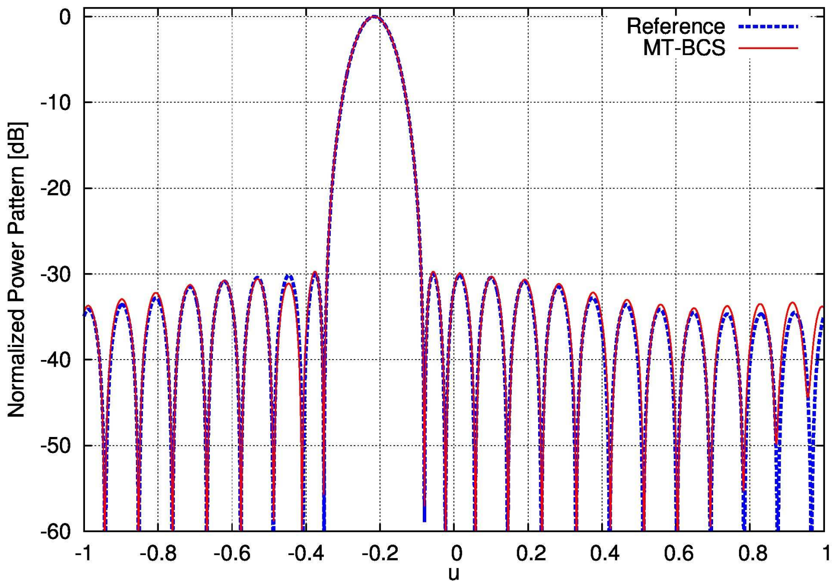

Figure 26: Power pattern comparison

Fig.25(a), *25*(b) show comparison between Reference and MT-BCS amplitudes and phases excitations respectively.

Fig.26 shows the comparison between Reference and MT-BCS power pattern for the steereng angle $\theta_5 = 102.46$ degrees.

	$SLL\,[dB]$	$D\,[dB]$	$HPBW\,[deg]$	M	err_5
$Reference$	-29.99	12.77	5.96	22	$-$
$MT-BCS$	-29.74	12.75	5.98	16	4.500321×10^{-1}

Table XV: Pattern $\theta_5$performance

In *Tab.*XV comparison between Reference and MT-BCS power pattern performance parameters.

Pattern $\theta_6 = 108.47\,deg$

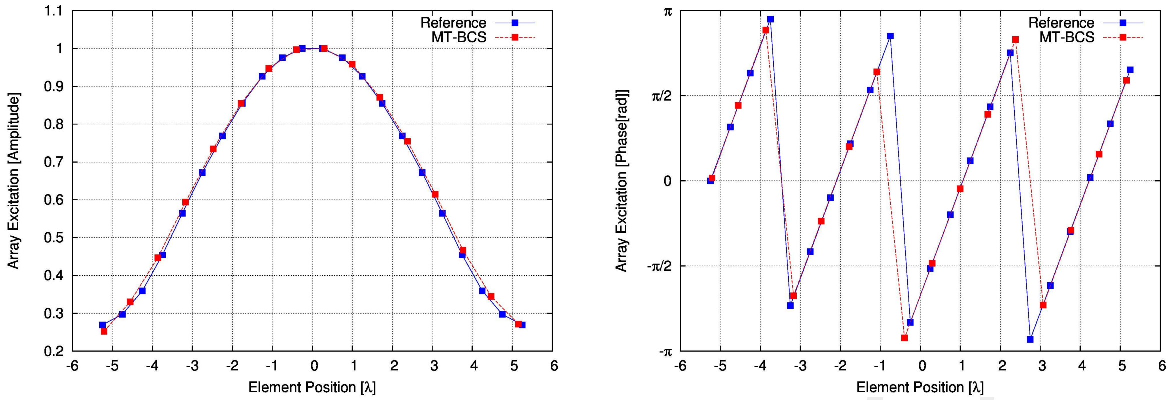

(a) (b)

Figure 27: Array Excitations, (a)Amplitudes, (b)Phases

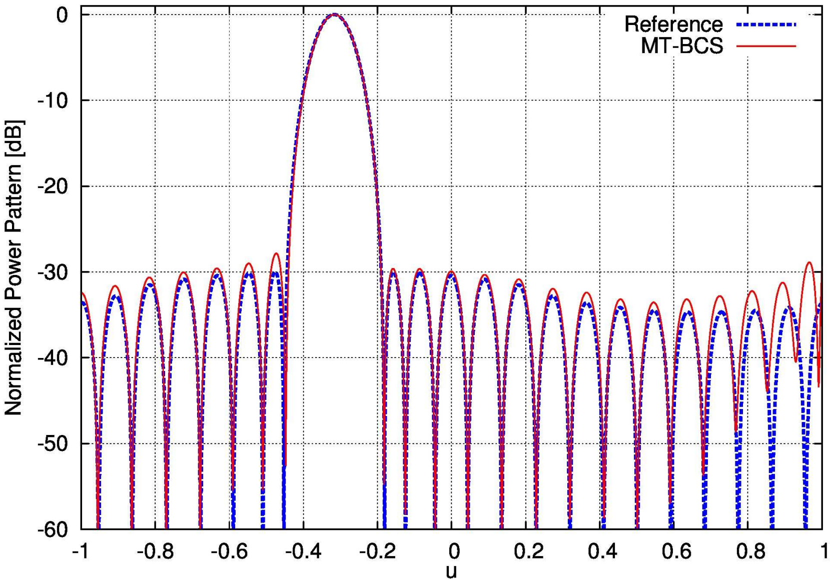

Figure 28: Power pattern comparison

Fig.27(a), *27*(b) show comparison between Reference and MT-BCS amplitudes and phases excitations respectively.

Fig.28 shows the comparison between Reference and MT-BCS power pattern for the steereng angle $\theta_6 = 108.47$ degrees.

	$SLL\,[dB]$	$D\,[dB]$	$HPBW\,[deg]$	M	err_6
$Reference$	-29.99	12.77	6.14	22	$-$
$MT-BCS$	-27.83	12.74	6.08	16	1.582593

Table XVI: Pattern $\theta_6$performance

In *Tab.*XVI comparison between Reference and MT-BCS power pattern performance parameters.

1.2.2 MT-BCS errors

In *Tab.*XVII are reported the error values. In particular:

- I: total number of reference power pattern $[I]$;
- ξ: total error of the entire procedure;
- err_i $(i = 1, \dots, I)$: error on sigular reference and MT-BCS pattern pair.

Solution	err_1	err_2	err_3	err_4	err_5	err_6
Best $M = 16$	4.677504×10^{-1}	3.633513×10^{-1}	3.678745×10^{-1}	3.926148×10^{-1}	4.500321×10^{-1}	1.582593

Solution	I	ξ
Best $M = 16$	6	6.040360×10^{-1}

Table XVII: MT-BCS errors

More information on the topics of this document can be found in the following list of references.

References

[1] P. Rocca, G. Oliveri, R. J. Mailloux, and A. Massa, "Unconventional phased array architectures and design Methodologies - A review," *Proceedings of the IEEE - Special Issue on 'Phased Array Technologies'*, Invited Paper, vol. 104, no. 3, pp. 544-560, March 2016.

[2] A. Massa, P. Rocca, and G. Oliveri, "Compressive sensing in electromagnetics - A review," *IEEE Antennas Propag. Mag.*, pp. 224-238, vol. 57, no. 1, Feb. 2015.

[3] F. Zardi, G. Oliveri, M. Salucci, and A. Massa, "Minimum-complexity failure correction in linear arrays via compressive processing," *IEEE Trans. Antennas Propag.*, vol. 69, no. 8, pp. 4504-4516, Aug. 2021.

[4] N. Anselmi, G. Gottardi, G. Oliveri, and A. Massa, "A total-variation sparseness-promoting method for the synthesis of contiguously clustered linear architectures" *IEEE Trans. Antennas Propag.*, vol. 67, no. 7, pp. 4589-4601, Jul. 2019.

[5] M. Salucci, A. Gelmini, G. Oliveri, and A. Massa, "Planar arrays diagnosis by means of an advanced Bayesian compressive processing," *IEEE Tran. Antennas Propag.*, vol. 66, no. 11, pp. 5892-5906, Nov. 2018.

[6] L. Poli, G. Oliveri, P. Rocca, M. Salucci, and A. Massa, "Long-Distance WPT Unconventional Arrays Synthesis" *J. Electromagn. Waves Appl.*, vol. 31, no. 14, pp. 1399-1420, Jul. 2017.

[7] G. Oliveri, M. Salucci, and A. Massa, "Synthesis of modular contiguously clustered linear arrays through a sparseness-regularized solver," *IEEE Trans. Antennas Propag.*, vol. 64, no. 10, pp. 4277-4287, Oct. 2016.

[8] M. Carlin, G. Oliveri, and A. Massa, "Hybrid BCS-deterministic approach for sparse concentric ring isophoric arrays," *IEEE Trans. Antennas Propag.*, vol. 63, no. 1, pp. 378-383, Jan. 2015.

[9] G. Oliveri, E. T. Bekele, F. Robol, and A. Massa, "Sparsening conformal arrays through a versatile BCS-based method," *IEEE Trans. Antennas Propag.*, vol. 62, no. 4, pp. 1681-1689, Apr. 2014.

[10] F. Viani, G. Oliveri, and A. Massa, "Compressive sensing pattern matching techniques for synthesizing planar sparse arrays," *IEEE Trans. Antennas Propag.*, vol. 61, no. 9, pp. 4577-4587, Sept. 2013.

[11] G. Oliveri, P. Rocca, and A. Massa, "Reliable diagnosis of large linear arrays - A Bayesian Compressive Sensing approach," *IEEE Trans. Antennas Propag.*, vol. 60, no. 10, pp. 4627-4636, Oct. 2012.

[12] G. Oliveri, M. Carlin, and A. Massa, "Complex-weight sparse linear array synthesis by Bayesian Compressive Sampling," *IEEE Trans. Antennas Propag.*, vol. 60, no. 5, pp. 2309-2326, May 2012.

[13] G. Oliveri and A. Massa, "Bayesian compressive sampling for pattern synthesis with maximally sparse non-uniform linear arrays," *IEEE Trans. Antennas Propag.*, vol. 59, no. 2, pp. 467-481, Feb. 2011.

[14] A. Benoni, P. Rocca, N. Anselmi, and A. Massa, "Hilbert-ordering based clustering of complex-excitations linear arrays," *IEEE Trans. Antennas Propag.*, vol. 70, no. 8, pp. 6751-6762, Aug. 2022.

[15] P. Rocca, L. Poli, N. Anselmi, and A. Massa, "Nested optimization for the synthesis of asymmetric shaped beam patterns in sub-arrayed linear antenna arrays," *IEEE Trans. Antennas Propag.*, vol. 70, no. 5, pp. 3385 - 3397, May 2022.

[16] P. Rocca, L. Poli, A. Polo, and A. Massa, "Optimal excitation matching strategy for sub-arrayed phased linear arrays generating arbitrary shaped beams," *IEEE Trans. Antennas Propag.*, vol. 68, no. 6, pp. 4638-4647, Jun. 2020.

[17] G. Oliveri, G. Gottardi and A. Massa, "A new meta-paradigm for the synthesis of antenna arrays for future wireless communications," *IEEE Trans. Antennas Propag.*, vol. 67, no. 6, pp. 3774-3788, Jun. 2019.

[18] P. Rocca, M. H. Hannan, L. Poli, N. Anselmi, and A. Massa, "Optimal phase-matching strategy for beam scanning of sub-arrayed phased arrays," *IEEE Trans. Antennas Propag.*, vol. 67, no. 2, pp. 951-959, Feb. 2019.

[19] N. Anselmi, P. Rocca, M. Salucci, and A. Massa, "Contiguous phase-clustering in multibeam-on-receive scanning arrays" *IEEE Trans. Antennas Propag.*, vol. 66, no. 11, pp. 5879-5891, Nov. 2018.

[20] L. Poli, G. Oliveri, P. Rocca, M. Salucci, and A. Massa, "Long-distance WPT unconventional arrays synthesis" *J. Electromagn. Waves Appl.*, vol. 31, no. 14, pp. 1399-1420, Jul. 2017.

[21] G. Gottardi, L. Poli, P. Rocca, A. Montanari, A. Aprile, and A. Massa, "Optimal monopulse beamforming for side-looking airborne radars," *IEEE Antennas Wirel. Propag. Lett.*, vol. 16, pp. 1221-1224, 2017.

[22] P. Rocca, M. D'Urso, and L. Poli, "Advanced strategy for large antenna array design with subarray-only amplitude and phase contr," *IEEE Antennas and Wirel. Propag. Lett.*, vol. 13, pp. 91-94, 2014.

[23] L. Manica, P. Rocca, G. Oliveri, and A. Massa, "Synthesis of multi-beam sub-arrayed antennas through an excitation matching strategy," *IEEE Trans. Antennas Propag.*, vol. 59, no. 2, pp. 482-492, Feb. 2011.

[24] M. Salucci, G. Oliveri, and A. Massa, "An innovative inverse source approach for the feasibility-driven design of reflectarrays," *IEEE Trans. Antennas Propag.*, vol. 70, no. 7, pp. 5468-5480, July 2022.

[25] L. T. P. Bui, N. Anselmi, T. Isernia, P. Rocca, and A. F. Morabito, "On bandwidth maximization of fixed-geometry arrays through convex programming," *J. Electromagn. Waves Appl.*, vol. 34, no. 5, pp. 581-600, 2020.

[26] N. Anselmi, L. Poli, P. Rocca, and A. Massa, "Design of simplified array layouts for preliminary experimental testing and validation of large AESAs," *IEEE Trans. Antennas Propag.*, vol. 66, no. 12, pp. 6906-6920, Dec. 2018.

[27] G. Oliveri and T. Moriyama, "Hybrid PS-CP technique for the synthesis of n-uniform linear arrays with maximum directivity" *J. Electromagn. Waves Appl.*, vol. 29, no. 1, pp. 113-123, Jan. 2015.

[28] P. Rocca and A. Morabito, “Optimal synthesis of reconfigurable planar arrays with simplified architectures for monopulse radar applications" *IEEE Trans. Antennas Propag.*, vol. 63, no. 3, pp. 1048-1058, Mar. 2015.

[29] A. F. Morabito and P. Rocca, “Reducing the number of elements in phase-only reconfigurable arrays generating sum and difference patterns," *IEEE Antennas Wireless Propag. Lett.*, vol. 14, pp. 1338-1341, 2015.

[30] P. Rocca, N. Anselmi, and A. Massa, “Optimal synthesis of robust beamformer weights exploiting interval analysis and convex optimization," *IEEE Trans. Antennas Propag.*, vol. 62, no. 7, pp. 3603-3612, Jul. 2014.

[31] G. Oliveri, G. Gottardi, M. A. Hannan, N. Anselmi, and L. Poli, "Autocorrelation-driven synthesis of antenna arrays - The case of DS-based planar isophoric thinned arrays," *IEEE Trans. Antennas Propag.*, vol. 68, no. 4, pp. 2895-2910, Apr. 2020.

[32] M. Salucci, G. Gottardi, N. Anselmi, and G. Oliveri, “Planar thinned array design by hybrid analytical-stochastic optimization," *IET Microw. Antennas Propag.*, vol. 11, no. 13, pp. 1841-1845, Oct. 2017

[33] T. Moriyama, E. Giarola, M. Salucci, and G. Oliveri, “On the radiation properties of ADS-thinned dipole arrays" *IEICE Electronics Express*, vol. 11, no. 16, pp. 1-10, Aug. 2014.

[34] G. Oliveri, F. Viani, and A. Massa, “Synthesis of linear multi-beam arrays through hierarchical ADS-based interleaving," *IET Microw. Antennas Propag.*, vol. 8, no. 10, pp. 794-808, Jul. 2014.

[35] D. Sartori, G. Oliveri, L. Manica, and A. Massa, “Hybrid Design of non-regular linear arrays with accurate control of the pattern sidelobes," *IEEE Trans. Antennas Propag.*, vol. 61, no. 12, pp. 6237-6242, Dec. 2013.